FULL PAPER

Dalton
www.rsc.org/dalton

Use of the di-2-pyridyl ketone/3,5-di-*tert*-butylcatechol "blend" in iron(III) chemistry: a cationic tetranuclear cluster and an anionic trinuclear complex †

Athanassios K. Boudalis,[a,b] Françoise Dahan,[a] Azzedine Bousseksou,[a] Jean-Pierre Tuchagues*[a] and Spyros P. Perlepes*[b]

[a] *Laboratoire de Chimie de Coordination du CNRS, UPR 8241, 205 route de Narbonne, 31077 Toulouse Cedex 04, France. E-mail: tuchague@lcc-toulouse.fr; Fax: +33-5-61553003; Tel: +33-5-61333154*

[b] *Department of Chemistry, University of Patras, 26504 Patras, Greece. E-mail: perlepes@patreas.upatras.gr; Fax: +30-2610-997118; Tel: +30-2610-997146*

Received 27th May 2003, Accepted 21st July 2003
First published as an Advance Article on the web 29th July 2003

The use of di-2-pyridyl ketone ($(py)_2CO$)/3,5-di-*tert*-butylcatechol (H_2dbcat) "blend" in iron(III) chemistry has yielded a cationic tetranuclear cluster and an anionic trinuclear complex. Both complexes were prepared under anaerobic conditions. The $Fe(ClO_4)_3\cdot 6H_2O$–$(py)_2CO$–H_2dbcat–NEt_3 (1 : 1 : 1 : 2) reaction system in MeOH gives $[Fe_4\{(py)_2C(OMe)O\}_2\{(Hpy)(py)C(OMe)O\}_2(dbcat)_4](ClO_4)_2$ **1**, whereas reaction of $Fe(ClO_4)_3\cdot 6H_2O$ with $(py)_2CO$, H_2dbcat and NEt_3 (1 : 1 : 1 : 3) in MeCN gives $(HNEt_3)[Fe_3\{(py)_2C(OH)O\}_2(dbcat)_4]\cdot$MeCN **2**·MeCN. The centrosymmetric tetranuclear cation of **1** contains a zigzag array of six-coordinate Fe^{III} ions. The inner Fe^{III} ions are bridged by two catecholate oxygen atoms from two $\eta^1{:}\eta^2{:}\mu_2$ $dbcat^{2-}$ groups, while one $\eta^1{:}\eta^2{:}\mu_2$ $dbcat^{2-}$ group and one $\eta^1{:}\eta^2{:}\eta^1{:}\mu_2$ $(py)_2C(OMe)O^-$ ligand bridge each inner Fe^{III} to its outer Fe^{III} neighbour. Each outer metal is chelated by a single bidentate $(^+Hpy)(py)C(OMe)O^-$ zwitterion. The trinuclear anion of **2**·MeCN consists of a triangular unit, in which the Fe_2 edges are bridged by two $\eta^1{:}\eta^2{:}\mu_2$ and one $\eta^1{:}\eta^2{:}\mu_3$ $dbcat^{2-}$ groups, and one $\eta^1{:}\eta^2{:}\eta^1{:}\mu_2$ $(py)_2C(OH)O^-$ ligand. Two Fe^{III} ions are six-coordinate, while the third is five-coordinate. One six-coordinate Fe^{III} centre is chelated by a bidentate $dbcat^{2-}$ group and the other one by a bidentate $(py)_2C(OH)O^-$ ligand. Variable-temperature magnetic susceptibility studies in the 2–300 K range reveal antiferromagnetic exchange interactions in both complexes. Variable-temperature Mössbauer spectra of **1** analyse as two quadrupole-split doublets which were assigned to the two different high-spin iron(III) sites in the complex, while those of **2** analyse as one (averaged) quadrupole-split doublet.

Introduction

Dinuclear and polynuclear iron(III) complexes have been of interest from a variety of viewpoints and have thus been intensely explored for many years. One field to which they are relevant is bioinorganic chemistry. Hydroxo- and oxo-bridged dinuclear complexes represent synthetic models of the active sites of various non-heme iron proteins, such as hemerythrin, methane monooxygenase and ribonucleotide reductase, the active sites of which have been shown to contain diiron cores bridged by oxo or hydroxo ligands.[1] The protein ferritin, which is involved in the storage and recycling of iron, has also received a great deal of attention.[2] It contains a symmetrical spherical cell consisting of 24 polypeptide units and can encapsulate up to *ca.* 4500 Fe ions in an iron oxide hydroxide core. A variety of polynuclear iron complexes have thus been prepared and studied as models for the buildup of the ferritin core.[3]

Another attractive aspect of polynuclear iron complexes is their potential to possess large spin (S) values in their ground state,[4] leading to the possible identification of iron-containing single-molecule magnets (SMMs).[5] SMMs[6] are molecular species which show a slow relaxation rate of the magnetization (of the order of months below 2 K) below a "blocking" temperature and they thus can function as tiny magnets of nanoscale dimensions. The unusual properties associated with SMMs require a combination of a relatively large S in the ground state with a considerable negative magnetic anisotropy; the origin of the latter is zero-field splitting (ZFS) in the ground state of a SMM arising from single-ion ZFS at the individual metal ions in the molecule. Although most complexes that function as SMMs identified to date are mixed-valence Mn species,[6,7] there are also a few iron(III) SMMs.[5] Iron(III) is an interesting metal ion to investigate in this field due to the five unpaired electrons (S = 5/2), a property which, for certain topologies, offers the potential to form high-spin clusters.[4] For the most intensively investigated iron(III) SMM, $[Fe_8O_2(OH)_2(tacn)_6]Br_8$ (S = 10, tacn = 1,4,7-triazacyclononane), the origin of the magnetic anisotropy responsible for the observed ZFS is a mixture of dipolar and single ion contributions.[6]

For both the above reasons we have recently developed an interest[8] in Fe_x cluster chemistry. In the present report, we describe two new Fe^{III} complexes, one trinuclear and one tetranuclear, isolated from the reaction of $Fe(ClO_4)_3\cdot 6H_2O$ with a ligand "blend" containing di-2-pyridyl ketone, $(py)_2CO$ and 3,5-di-*tert*-butylcatechol, H_2dbcat, see Scheme 1.

We[9,10] and others[11] have found that the anions of the *gem*-diol form of $(py)_2CO$ are excellent sources of polynuclear Mn^{II}, $Mn^{II/III}$, Co^{II}, Ni^{II} and Cu^{II} complexes with aesthetically pleasing structures, rare nuclearities (M_5, M_7, M_8, M_9, M_{12}, M_{14}) and interesting magnetic properties (*e.g.* high-spin molecules). The immense structural diversity displayed by the complexes reported stems from the ability of the doubly and singly deprotonated ions of the *gem*-diol form of $(py)_2CO$, $(py)_2CO_2^{2-}$ and $(py)_2C(OH)O^-$, respectively, or the monoanion of the hemiacetal form of the ligand, $(py)_2C(OR)O^-$, to exhibit no less than nine distinct coordination modes; these three anions (Scheme 1) do not exist as free species but exist only in their complexes. It is noteworthy that only one mononuclear iron(III) complex containing the tridentate chelating $(py)_2C(OH)O^-$ ligand, namely $[Fe\{(py)_2C(OH)O\}_2](NO_3)\cdot 2H_2O$, has been structurally characterized to date.[12]

† Electronic supplementary information (ESI) available: Mössbauer spectra of complex **2** at 80, 150 and 293 K. See http://www.rsc.org/suppdata/dt/b3/b305873e/

DOI: 10.1039/b305873e

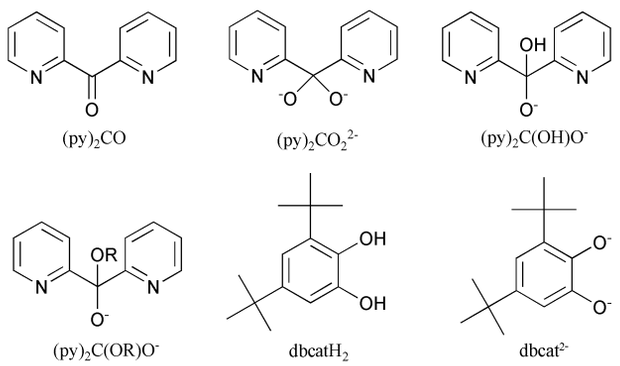

Scheme 1 Some of the ligands discussed in the text; note that $(py)_2CO_2^{2-}$, $(py)_2C(OH)O^-$ and $(py)_2C(OR)O^-$ do not exist as free species but they exist only in their metal complexes.

Interest in the chemistry of transition metal catecholate complexes has greatly increased in recent years.[13] One reason for this has been the charge distribution in metal *o*-benzoquinone systems.[14] The localized quinonoid (quinone, semiquinone or catechol) electronic levels in metal complexes are close in energy to the metal electronic levels. The ordering of these levels affects the oxidation state of the metal and the quinone *via* the intramolecular transport scheme represented by eqn. (1),

$$M^{n-1}(Q^0) \rightleftharpoons M^n(SQ^-) \rightleftharpoons M^{n+1}(Cat^{2-}) \qquad (1)$$

where Q = benzoquinone, SQ^- = benqosemiquinonate and Cat^{2-} = catecholate.[15,16] Another reason for the great research activity in the coordination chemistry of catechols and semiquinones has been the recognition of the important roles of these ligands in biology.[17] In particular, iron(III) catecholate chemistry has been extensively studied because of its relevance to bacterial siderophores, biologically important catecholamines, the intradiol-cleaving enzyme catechol 1,2-dioxygenase and to DOPA containing proteins.[18,19] Catecholate(−2) ions normally act as bidentate chelating ligands,[20] but doubly-[13,15,16] or triply-bridging[15] coordination behaviours are by no means rare, thus favouring cluster formation.[15,16]

The great coordinative flexibility and versatility of the $(py)_2CO$-based anionic ligands (presumably due to the presence of dissimilar atoms within the ligands), and the μ_2 or μ_3 potential of catecholate(−2) ligands, prompted us to combine the two ligand systems to aim for new polynuclear complexes. Our belief was that the simultaneous employment of both classes of ligands in high-nuclearity 3d-metal chemistry would give an extraordinary structural flexibility in the mixed ligand systems ("blends"). The loss of a degree of the synthetic control[21] would be more than compensated for by the vast diversity of structures expected using the combination of ligands. The present report represents our first effort along this line. This work is a next step in a broad programme[8–10,22] concerned with developing synthetic routes to, and studying the magnetic properties of, polynuclear complexes of 3d metals at intermediate oxidation states.

Experimental

Syntheses

All reagents were used as received. All complexation reactions and sample preparations for physical measurements were carried out in a purified nitrogen atmosphere within a glovebox (Vacuum Atmospheres H.E.43.2) equipped with a dry train (Jahan EVAC 7). All solvents were degassed prior to use.

$[Fe_4\{(py)_2C(OMe)O\}_2\{(Hpy)(py)C(OMe)O\}_2(dbcat)_4](ClO_4)_2$ (1). A solution of $(py)_2CO$ (0.184 g, 1.00 mmol) in MeOH (5 mL) was added to a solution of $Fe(ClO_4)_3{\cdot}6H_2O$ (0.462 g, 1.00 mmol) in the same solvent (5 mL). The resulting orange solution was stirred while a methanolic solution (5 mL) containing H_2dbcat (0.222 g, 1.00 mmol) and NEt_3 (0.278 mL, 2.00 mmol) was added. A noticeable colour change to dark blue occurred and the reaction solution was allowed to stand uncovered at room temperature. After 2 days, blue–black cubic crystals of **1** of crystallographic quality were separated by filtration from the dark solution, washed with MeOH and dried *in vacuo*. The yield was 60%. Anal. Calc. (Found) for $C_{104}H_{126}Cl_2Fe_4N_8O_{24}$: C, 57.66 (57.30); H, 5.86 (5.98); N, 5.17 (5.04)%. IR data (KBr, cm^{-1}): 3091m, 2950vs, 2904m, 2865s, 1604s 1519w, 1471m, 1460m, 1439m, 1408w, 1386w, 1359w, 1278m, 1255m, 1227m, 1108vs, 1090vsb, 1060vs, 1049vs, 1025s, 974s, 861w, 833w, 788m, 765s, 686m, 624m, 572w, 482m, 467m, 420w.

$(HNEt_3)[Fe_3\{(py)_2C(OH)O\}_2(dbcat)_4]{\cdot}MeCN$ (2·MeCN). An orange solution of $Fe(ClO_4)_3{\cdot}6H_2O$ (0.277 g, 0.60 mmol) and $(py)_2CO$ (0.110 g, 0.60 mmol) in MeCN (8 mL) was treated with a solution of H_2dbcat (0.133 g, 0.60 mmol) and NEt_3 (0.250 mL, 1.80 mmol) in the same solvent (8 mL) to give a colour change to dark blue. After being stirred for 10 min, the resulting solution was allowed to stand covered at room temperature for one week and blue–black, parallelepiped-shaped crystals of **2**·MeCN were obtained. The crystals were collected by filtration, rinsed with a small amount of MeCN and dried *in vacuo*. The yield was 45%. The crystals turn to powder on drying; a fully dried sample analysed as solvent-free. Anal. Calc. (Found) for $C_{84}H_{114}Fe_3N_5O_{12}$: C, 58.40 (58.27); H, 4.32 (4.40); N, 6.28 (6.19)%. IR data (KBr, cm^{-1}): 2950vs, 2903s, 2866s, 1603w, 1570w, 1476m, 1438s, 1410m, 1360w, 1281m, 1236mb, 1207m, 1157m, 1126s, 1090s, 1045s, 985s, 860w, 830w, 763s, 688m, 651m, 589m, 491m.

Crystallographic data collection and structure determination for 1 and 2

The crystallographic data together with the refinement details for **1** and **2**·MeCN are summarized in Table 1. The selected crystals of **1** (black block, 0.25 × 0.25 × 0.15 mm) and **2**·MeCN (dark-blue parallelepiped, 0.35 × 0.25 × 0.20 mm) were mounted on a Stoe Imaging Plate Diffractometer System (IPDS) equipped with an Oxford Cryosystems cooler device

Table 1 Crystallographic data for complexes **1** and **2**

	1	**2**·MeCN
Formula	$C_{104}H_{126}Cl_2Fe_4N_8O_{24}$	$C_{86}H_{117}Fe_3N_6O_{12}$
M_w	2166.43	1594.41
Crystal system	Triclinic	Monoclinic
Space group	$P\bar{1}$ (no. 2)	$P2_1/c$ (no. 14)
a/Å	11.2904(11)	21.495(2)
b/Å	15.3440(17)	18.6521(13)
c/Å	17.2747(16)	23.326(3)
α/°	99.013(12)	90.0
β/°	101.928(11)	112.586(14)
γ/°	108.254(12)	90.0
V/Å^3	2700.6(5)	8634.8(16)
Z	1	4
F(000)	1136	3396
T/K	180	160
λ/Å	0.71073	0.71073
D_c/Mg m^{-3}	1.332	1.226
μ(Mo-Kα)/mm^{-1}	0.649	0.558
Meas./indep. refl.	26615/9838	67360/17043
Obs. refl. [$F > 4\sigma(F)$]	7159	10336
$wR(F^2)^b$	0.0691	0.0932
R^a [$F > 4\sigma(F)$]	0.0351	0.0436
Goodness of fit on F^2	0.878	0.854
$\Delta\rho_{max,\ min}$/e A^{-3}	0.595, −0.290	0.685, −0.513

^{a} $R = \Sigma||F_o| - |F_c||/\Sigma|F_o|$. ^{b} $wR = [\Sigma w(|F_o^2| - |F_c^2|)^2/\Sigma w|F_o^2|^2]^{1/2}$.

at 180 K for **1** and 160 K for **2**·MeCN using a graphite monochromator (λ = 0.71073 Å). The crystal-to-detector distance was 70 mm (max 2θ value 52.1°). Data were collected with a φ oscillation movement (φ = 0.0–249.0°, $\Delta\varphi$ = 1.5° for **1**, φ = 0.0–200.2°, $\Delta\varphi$ = 1.4° for **2**·MeCN). 26615 Reflections of which 9838 independent (R_{int} = 0.0381) for **1** and 67360 reflections of which 17043 independent (R_{int} = 0.0535) for **2**·MeCN were collected. Numerical absorption[23] corrections were applied for **1** (T_{max} = 0.8319, T_{min} = 0.6806). The structures were solved by direct methods using SHELXS-97[24] and refined by full-matrix least-squares on F_o^2 with SHELXL-97[25] with anisotropic displacement parameters for all non-hydrogen atoms. H atoms were introduced in calculations using the riding model with isotropic thermal parameters 1.1 times higher than those of the riding atom. Scattering factors were taken from ref. 26. The molecular plots were obtained using the ORTEP32 program.[27]

CCDC reference number 211396 for **1** and 211397 for **2**·MeCN.

See http://www.rsc.org/suppdata/dt/b3/b305873e/ for crystallographic data in CIF or other electronic format.

Physical measurements

Elemental analyses (C, H, N) were performed by the Microanalytical Laboratory of the Laboratoire de Chimie de Coordination du CNRS at Toulouse. Infrared spectra were recorded in the solid state (KBr pellets) on a Perkin-Elmer 16PC spectrometer in the 4000–400 cm^{-1} range. Variable-temperature (2–300 K) magnetic susceptibility measurements were performed on a Quantum Design MPMS SQUID susceptometer at magnetic fields of 1.0 (complex **1**) and 0.75 T (complex **2**). Samples were 3 mm diameter pellets moulded in the glovebox from ground crystalline samples. Pascal's constants were used to estimate the diamagnetic corrections. The magnetic susceptibility has been computed by exact calculation of the energy levels associated with the spin Hamiltonian through diagonalization of the full matrix with a general program for axial symmetry.[28] Least-squares fittings were accomplished with an adapted version of the function-minimization program MINUIT.[29] Mössbauer measurements were recorded on a constant acceleration conventional spectrometer with a 50 mCi source of ^{57}Co (Rh matrix). The absorber was a powdered sample enclosed in a 20 mm diameter cylindrical, plastic sample-holder, the size of which had been determined to optimize the absorption. Variable-temperature spectra were obtained in the 6–300 K range, by using a MD 306 Oxford cryostat, the thermal scanning being monitored by an Oxford ITC4 servocontrol device (± 0.1 K accuracy). The Recoil program package[30] was used to fit the Mössbauer parameters and determine their standard deviations of statistical origin (given in parentheses). Isomer shift values (δ) are reported relative to iron foil at 293 K.

Results and discussion

Syntheses

Complexes **1** and **2** were obtained using the $Fe(ClO_4)_3{\cdot}6H_2O$–$(py)_2CO$–H_2dbcat–NEt_3 reaction system in MeOH (1 : 1 : 1 : 2) and MeCN (1 : 1 : 1 : 3), respectively. Their formation can be summarized in balanced eqns. (2) and (3).

$$4\ Fe(ClO_4)_3{\cdot}6H_2O + 4\ (py)_2CO + 4\ H_2dbcat + 4\ MeOH + 8\ NEt_3 \xrightarrow{MeOH} [Fe_4\{(py)_2C(OMe)O\}_2\{(Hpy)(py)C(OMe)O\}_2(dbcat)_4](ClO_4)_2 \quad \mathbf{1} \quad + 8\ HNEt_3ClO_4 + 2\ HClO_4 + 24\ H_2O \qquad (2)$$

$$3\ Fe(ClO_4)_3{\cdot}6H_2O + 2\ (py)_2CO + 4\ H_2dbcat + 10\ NEt_3 \xrightarrow{MeCN} (HNEt_3)[Fe_3\{(py)_2C(OH)O\}_2(dbcat)_4] \quad \mathbf{2} \quad + 9\ HNEt_3ClO_4 + 16\ H_2O \qquad (3)$$

The iron(III)-mediated addition of solvent (MeOH, H_2O involved in MeCN and starting materials) to $(py)_2CO$ to give the neutral zwitterionic, $(^+Hpy)(py)C(OMe)O^-$, and monoanionic, $(py)_2C(OMe)O^-$, forms of the hemiacetal $(py)_2C(OMe)(OH)$ (Scheme 1, R = Me) in **1** and the monoanion $(py)_2C(OH)O^-$ (Scheme 1) in **2** involves a nucleophilic attack of the ROH molecule (R = Me, H) on the carbonyl group.[9] The electrophilic character of the carbonyl carbon atom of $(py)_2CO$ is increased by coordination of the carbonyl oxygen to the metal ion (direct polarization) or/and by coordination of the more remote 2-pyridyl sites (induced polarization).[31]

The "wrong" stoichiometry employed for the preparation of **2** compared to that required by eqn. (3) obviously did not prove detrimental to the formation of the anionic Fe_3 product. With the identity of **2** established crystallographically, a higher-yield (~60%) preparative route (not reported in Experimental section) was devised by adjusting the Fe^{III} : $(py)_2CO$: H_2dbcat : NEt_3 reaction ratio to 1.5 : 1 : 2 : 5.

A final point of synthetic interest is the strict absence of oxygen from the reaction mixtures that lead to **1** and **2**. The anaerobic conditions aimed at protecting the $dbcat^{2-}$ ligand from an intradiol cleavage caused by a possible iron(III) active intermediate that might form in solution in the presence of oxygen.[13,15,17]

Description of structures

ORTEP representations of the ions of complexes **1** and **2**·MeCN are shown in Figs. 1 and 2, respectively. Selected interatomic distances and angles are listed in Tables 2 and 3.

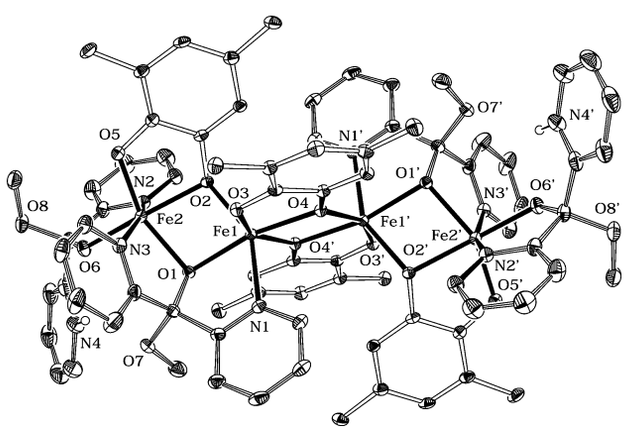

Fig. 1 ORTEP representation of the cation of complex **1** with the atoms drawn at the 30% probability level. Primes are used for symmetry-related atoms. Most hydrogen atoms and all methyl carbon atoms of the *tert*-butyl groups have been omitted for clarity.

Complex **1** crystallizes in triclinic space group $P\bar{1}$. Its structure consists of the centrosymmetric tetranuclear $[Fe_4\{(py)_2C(OMe)O\}_2\{(Hpy)(py)C(OMe)O\}_2(dbcat)_4]^{2+}$ cation and ClO_4^- anions; the latter will not be further discussed. The cation contains an almost linear array of Fe^{III} atoms and has an $[Fe_4(\mu_2\text{-}OR)_4(\mu_2\text{-}OR')_2]^{6+}$ core (R = $OC_6H_2(CMe_3)_2$–; R′ = $(py)_2C(OMe)$–). The core can be conveniently described as consisting of two $\{Fe_2(\mu\text{-}OR)(\mu\text{-}OR')\}^{4+}$ units doubly bridged by two catecholate oxygen atoms. The bridging system comprises four $\eta^1{:}\eta^2{:}\mu_2$ (or 2.12 using Harris notation[32]) $dbcat^{2-}$ groups and two $\eta^1{:}\eta^2{:}\eta^1{:}\mu_2$ (or 2.211 using Harris notation[32]) $(py)_2C(OMe)O^-$ ligands. According to Harris notation,[32] the binding mode of a ligand is referred to as $X.Y_1Y_2Y_3\cdots Y_n$, where X is the overall number of metals

Table 2 Selected bond lengths (Å) and angles (°) for complex **1**[a]

Fe(1)–O(1)	2.0820(14)	Fe(2)–O(1)	2.0570(14)
Fe(1)–O(2)	2.0363(13)	Fe(2)–O(2)	2.0698(14)
Fe(1)–O(3)	1.9020(13)	Fe(2)–O(5)	1.8923(14)
Fe(1)–O(4)	2.0791(14)	Fe(2)–O(6)	1.9460(15)
Fe(1)–O(4′)	2.0045(13)	Fe(2)–N(2)	2.1576(17)
Fe(1)–N(1)	2.1576(16)	Fe(2)–N(3)	2.1444(17)
Fe(1) ··· Fe(2)	3.1992(5)	Fe(1) ··· Fe(1′)	3.2983(7)
O(1)–Fe(1)–O(2)	76.57(5)	O(1)–Fe(2)–O(2)	76.39(5)
O(1)–Fe(1)–O(3)	104.29(6)	O(1)–Fe(2)–O(5)	149.13(6)
O(1)–Fe(1)–O(4)	168.15(5)	O(1)–Fe(2)–O(6)	103.79(6)
O(1)–Fe(1)–O(4′)	103.91(5)	O(1)–Fe(2)–N(2)	106.63(6)
O(1)–Fe(1)–N(1)	74.99(6)	O(1)–Fe(2)–N(3)	75.36(6)
O(2)–Fe(1)–O(3)	88.28(6)	O(2)–Fe(2)–O(5)	81.61(6)
O(2)–Fe(1)–O(4)	114.98(5)	O(2)–Fe(2)–O(6)	164.37(6)
O(2)–Fe(1)–O(4′)	100.55(5)	O(2)–Fe(2)–N(2)	87.66(6)
O(2)–Fe(1)–N(1)	148.79(6)	O(2)–Fe(2)–N(3)	109.50(6)
O(3)–Fe(1)–O(4)	79.61(5)	O(5)–Fe(2)–O(6)	103.20(7)
O(3)–Fe(1)–O(4′)	151.69(6)	O(5)–Fe(2)–N(2)	93.68(6)
O(3)–Fe(1)–N(1)	86.52(6)	O(5)–Fe(2)–N(3)	92.23(6)
O(4)–Fe(1)–O(4′)	72.27(6)	O(6)–Fe(2)–N(2)	77.26(6)
O(4)–Fe(1)–N(1)	94.27(6)	O(6)–Fe(2)–N(3)	85.36(6)
O(4′)–Fe(1)–N(1)	98.50(6)	N(2)–Fe(2)–N(3)	162.51(7)
Fe(1)–O(1)–Fe(2)	101.24(6)	Fe(1)–O(2)–Fe(2)	102.36(6)
Fe(1)–O(4)–Fe(1′)	107.73(6)		

[a] Symmetry code: (′) = 1 − *x*, 1− *y*, 1− *z*.

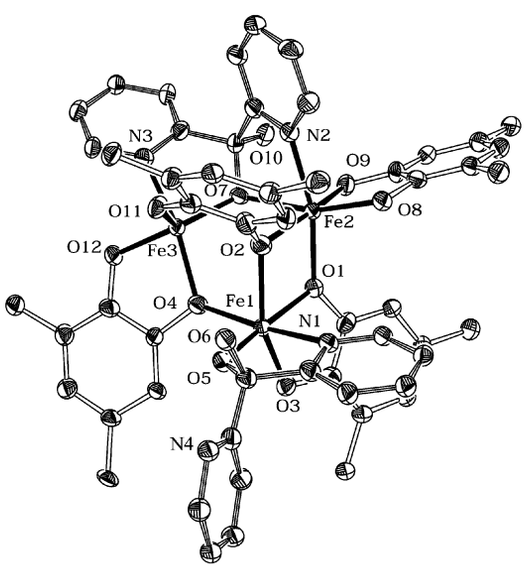

Fig. 2 ORTEP representation of the anion of complex **2**·MeCN with the atoms drawn at the 30% probability level. Hydrogen atoms and methyl carbon atoms of the *tert*-butyl groups have been omitted for clarity.

bound by the whole ligand and each value of Y refers to the number of metal ions attached to the different donor atoms. The ordering of Y is listed by the Cahn–Ingold–Prelog priority rules, hence here O before N. The inner Fe^{III} atoms (Fe(1), Fe(1′)) are bridged by two catecholate oxygen atoms ((O4), O(4′)), while one $dbcat^{2-}$ group and one $(py)_2C(OMe)O^-$ ligand bridge each inner Fe^{III} to its outer Fe^{III} neighbour. Each outer metal ion (Fe(2), Fe(2′)) is chelated by a single ($^+$Hpy)(py)-C(OMe)O^- zwitterion bound in a bidentate (η^1:η^1, 1.11) fashion and forming a five-membered ring. The coordination modes of the ligands present in **1**, and the Harris notation to describe these modes, are shown in Scheme 2.

The central Fe(1)O(4)Fe(1′)O(4′) core is strictly planar due to the presence of an inversion centre in the middle of the core, with an Fe(1)–O(4)–Fe(1′) angle of 107.7° and an Fe(1) ··· Fe(1′) separation of 3.298 Å. The external $\{Fe_2(\mu\text{-OR})(\mu\text{-OR}')\}^{4+}$ units exhibit smaller Fe–O–Fe angles (Fe(1)–O(1)–Fe(2), 101.2°; Fe(1)–O(2)–Fe(2), 102.4°) and a slightly shorter metal–metal separation (Fe(1) ··· Fe(2), 3.199 Å); in addition, these units are not planar, the torsion angle Fe(1)–O(1)–Fe(2)–O(2) being 14.0°.

Table 3 Selected bond lengths (Å) and angles (°) for complex **2**·MeCN

Fe(1)–O(1)	2.0486(13)	Fe(2)–O(1)	1.9811(13)
Fe(1)–O(2)	2.0992(14)	Fe(2)–O(2)	2.0490(14)
Fe(1)–O(3)	1.9280(14)	Fe(2)–O(7)	2.1364(14)
Fe(1)–O(4)	1.9915(14)	Fe(2)–O(8)	1.9250(14)
Fe(1)–O(5)	1.9104(14)	Fe(2)–O(9)	1.9547(14)
Fe(1)–N(1)	2.1999(17)	Fe(2)–N(2)	2.1373(16)
Fe(3)–O(4)	2.0226(14)	Fe(3)–O(11)	1.8603(14)
Fe(3)–O(7)	2.0015(12)	Fe(3)–O(12)	1.9103(13)
Fe(3)–N(3)	2.1980(18)	Fe(1) ··· Fe(2)	3.2799(3)
Fe(2) ··· Fe(3)	3.4409(3)	Fe(1) ··· Fe(3)	3.4107(3)
O(1)–Fe(1)–O(2)	72.02(5)	O(1)–Fe(2)–O(2)	74.46(5)
O(1)–Fe(1)–O(3)	80.64(6)	O(1)–Fe(2)–O(7)	96.57(5)
O(1)–Fe(1)–O(4)	94.96(6)	O(1)–Fe(2)–O(8)	100.41(6)
O(1)–Fe(1)–O(5)	167.62(6)	O(1)–Fe(2)–O(9)	100.42(6)
O(1)–Fe(1)–N(1)	90.42(6)	O(1)–Fe(2)–N(2)	163.74(6)
O(2)–Fe(1)–O(3)	152.65(6)	O(2)–Fe(2)–O(7)	80.52(5)
O(2)–Fe(1)–O(4)	80.99(6)	O(2)–Fe(2)–O(8)	108.95(6)
O(2)–Fe(1)–O(5)	102.58(6)	O(2)–Fe(2)–O(9)	166.14(6)
O(2)–Fe(1)–N(1)	89.93(6)	O(2)–Fe(2)–N(2)	90.38(6)
O(3)–Fe(1)–O(4)	101.25(6)	O(7)–Fe(2)–O(8)	162.25(5)
O(3)–Fe(1)–O(5)	104.34(6)	O(7)–Fe(2)–O(9)	87.41(5)
O(3)–Fe(1)–N(1)	90.82(6)	O(7)–Fe(2)–N(2)	74.71(5)
O(4)–Fe(1)–O(5)	95.15(6)	O(8)–Fe(2)–O(9)	84.51(6)
O(4)–Fe(1)–N(1)	167.44(6)	O(8)–Fe(2)–N(2)	89.93(6)
O(5)–Fe(1)–N(1)	78.29(6)	O(9)–Fe(2)–N(2)	92.98(6)
O(4)–Fe(3)–O(7)	99.15(5)	O(7)–Fe(3)–O(12)	130.55(6)
O(4)–Fe(3)–O(11)	110.75(6)	O(7)–Fe(3)–N(3)	77.37(6)
O(4)–Fe(3)–O(12)	81.07(6)	O(11)–Fe(3)–O(12)	104.45(6)
O(4)–Fe(3)–N(3)	149.79(6)	O(11)–Fe(3)–N(3)	96.16(6)
O(7)–Fe(3)–O(11)	120.76(6)	O(12)–Fe(3)–N(3)	79.04(6)
Fe(1)–O(1)–Fe(2)	108.96(6)	Fe(1)–O(2)–Fe(2)	104.50(6)
Fe(2)–O(7)–Fe(3)	112.48(6)		

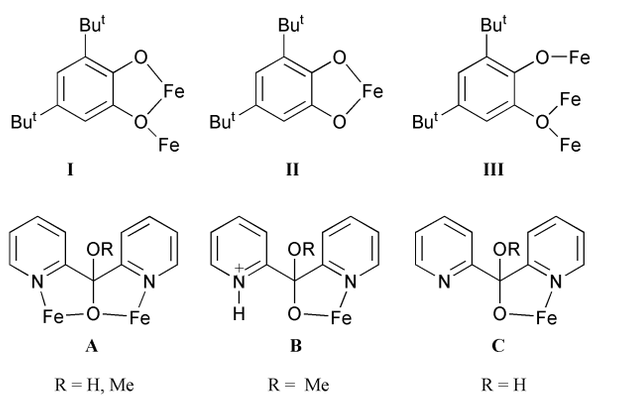

Scheme 2 The crystallographically established coordination modes of the ligands present in complexes **1** and **2**·MeCN, and the Harris notation[32] that describes these modes.

The Fe^{III} ions are both octahedrally coordinated, their chromophores being $Fe(1)NO_5$ and $Fe(2)N_2O_4$. Inspection of the bond angle values listed in Table 2 clearly shows that deviation from octahedral geometry is more pronounced in the case of Fe(1).

The Fe–N and Fe–O bond lengths agree well with values expected for high-spin iron(III).[20] The bridging Fe–O distances are asymmetric. The Fe–O bond distances for the bridging catecholate oxygen atoms are longer than the Fe–O distance exhibited by the terminal oxygen atom from the same catecholate unit. For example, the Fe(1)–O(4) and Fe(1′)–O(4) bond distances are 2.079 and 2.004 Å, respectively, while the Fe(1)–O(3) distance is 1.902 Å. The increase in bond length upon bridging relative to terminal ligation has been observed previously[13,15] in many complexes containing catecholate(2−) ligands with one bridging oxygen, including the complex $[Fe_4(dbsq)_4(dbcat)_4]$, which exhibits three coordination modes for the catecholate oxygen, *viz.*, terminal, μ_2 and μ_3 with average bond lengths of 1.868, 2.000 and 2.183 Å, respectively.[16]

The $dbcat^{2-}$ C–O bond distances in **1** display a pattern similar to those in $[Fe_4(dbsq)_4(dbcat)_4]$.[16] Thus, the terminal C–O bond lengths in **1** (average 1.341 Å) are shorter than those observed for the bridging groups (average 1.370 Å). The bridging oxygen O(4) has a planar coordination (Σ°O(4) = 360°), while the coordination of the remaining bridging oxygen (O(2)) is somewhat pyramidal (Σ°O(2) = 337.5°). The average OC–CO ring distance for the two crystallographically independent $dbcat^{2-}$ ligands of **1** is 1.409 Å.

C–O distances are considered diagnostic of the oxidation state of 1,2-benzodioxy ligands.[13–15] Catecholate C–O distances are generally in the range 1.34–1.39 Å, those of semiquinonates are shorter at 1.28–1.31 Å, and quinone C–O distances are shortest at ~1.23 Å. OC–CO ring distances follow the reverse pattern, with catecholates having much shorter C–C distances (~1.40 Å) than quinones (~1.50 Å). In the present case, the C–O and OC–CO bond distances are both characteristic for catecholato ligation rather than semiquinonato or quinone ligation.[13,15]

An intramolecular hydrogen bond is present in **1** with the protonated 2-pyridyl nitrogen, N(4), as donor and the uncoordinated oxygen of $(py)_2C(OMe)O^-$, O(7), as acceptor; its dimensions are N(4) ··· O(7) (1 − *x*, 1 − *y*, 1 − *z*) 3.107(3) Å, H ··· O(7) (1 − *x*, 1 −*y*, 1 − *z*) 2.37 Å and N(4)–H ··· O(7) (1 − *x*, 1 − *y*, 1 − *z*) 141.1°.

Complex **2** crystallizes in monoclinic space group $P2_1/c$. Its structure consists of the trinuclear $[Fe_3\{(py)_2C(OH)O\}_2(dbcat)_4]^-$ anion, one $HNEt_3^+$ cation and one solvate MeCN molecule; the latter two will not be further discussed. The anion has no crystallographically imposed symmetry and consists of a triangular unit containing a $[Fe_3(\mu_2\text{-}OR)(\mu_2\text{-}OR')]^{5+}$ core (R = $OC_6H_2(CMe_3)_2$–; R′ = $(py)_2C(OH)$–). At first glance, one might consider that the three Fe^{III} ions are located at three corners of a defective cubane (a cubane missing one vertex). However, the Fe(3)–O(2) separation (2.573 Å) is too long to be considered as a bonding interaction and, thus, this description is not realistic. The Fe_2 edges are bridged by a total of four groups, two of which are $dbcat^{2-}$ ligands in the $\eta^1{:}\eta^2{:}\mu_2$ (or 2.12 using Harris notation) manner, one is an $\eta^1{:}\eta^2{:}\mu_3$ (3.12) $dbcat^{2-}$ ligand and the fourth an $\eta^1{:}\eta^2{:}\eta^1{:}\mu_2$ (2.211) $(py)_2C(OH)O^-$ ion. The single μ_3 $dbcat^{2-}$ ligand is that involving O(2) and O(11). Six-coordination at Fe(1) and Fe(2) is completed by a chelating $\eta^1{:}\eta^1$ (1.11) $(py)_2C(OH)O^-$ ion and a chelating $\eta^1{:}\eta^1$ (1.11) $dbcat^{2-}$ group, respectively, both forming five-membered rings. The coordination modes of the ligands present in **2** are shown in Scheme 2. The presence of two monoatomic bridges (O(1), O(2)) between Fe(1) and Fe(2) causes the Fe_3 triangle to be vitrually isosceles with the Fe(1) ··· Fe(2) separation (3.280 Å) being significantly shorter than Fe(1) ··· Fe(3) (3.411 Å) and Fe(2) ··· Fe(3) (3.441 Å).

Fe(1) and Fe(2) have distorted octahedral geometries; both are bound to an NO_5 donor set. The five donor atoms within bonding distances do not define a regular polyhedron around Fe(3). Analysis of the shape determining angles using the approach of Addison, Reedijk and co-workers[33] yields a value for trigonality index, τ, of 0.32 (τ = 0 and 1 for perfect square pyramidal and trigonal bipyramidal geometries, respectively). Thus, the geometry about Fe(3) is significantly distorted. With the use of the more preferred TBPY description, the axial sites are occupied by atoms O(4) and N(3) with atoms O(7), O(11) and O(12) making up the equatorial plane.

The Fe–N lengths of $[Fe\{(py)_2C(OH)O\}_2](NO_3)\cdot 2H_2O$[12] (average 1.951 Å) are significantly shorter than those in **2**·MeCN (average 2.178 Å); similarly, the terminal Fe(1)–O(5) length in **2**·MeCN (1.910 Å) is sligthly longer than corresponding parameters in the mononuclear complex (average 1.862 Å). The shortened Fe–N and terminal Fe–O bonds in $[Fe\{(py)_2C(OH)O\}_2](NO_3)\cdot 2H_2O$ *vs.* **2**·MeCN may both reasonably be attributed to the *tridentate* chelating nature of $(py)_2C(OH)O^-$ in the mononuclear complex.

The bridging Fe–O distances are all symmetric (for example, Fe(1)–O(1) 2.049 and Fe(2)–O(1) 1.981 Å) and longer than the six terminal Fe–O distances (1.860–1.955 Å). The three catecholate bridging oxygens (O(1), O(2), O(4)) are essentially planar (Σ°O = 354.4–357.8°); in contrast, the $(py)_2C(OH)O^-$ bridging oxygen is somewhat pyramidal (Σ°O(7) = 339.7°). The $dbcat^{2-}$ C–O distances are shorter for the terminal oxygens (1.327–1.361 Å) than those for the bridging ones (1.375–1.361 Å), while the OC–CO ring distances are in the range 1.406–1.438 Å. Almost all these distances fall into the ranges expected for the catecholate, rather than semiquinonate ligands.[13,15]

The crystal structure of **2**·MeCN is stabilized by hydrogen bonds involving the uncoordinated oxygen of the $\eta^1{:}\eta^2{:}\eta^1{:}\mu_2$ $(py)_2C(OH)O^-$ ligand, O(10), and the protonated nitrogen of $HNEt_3^+$, N(5), as donors and one of the oxygens (O(9)) of the chelating $dbcat^{2-}$ group and uncoordinated atoms N(4) and O(6) of the chelating $(py)_2C(OH)O^-$ ligand as acceptors.

Ligands based on the *gem*-diol or the hemiacetal forms of di-2-pyridyl ketone have been observed in numerous ligation modes over the years,[9,11] but the particular bidentate chelating (1.11) coordination modes (Scheme 2) observed for $(^+Hpy)(py)C(OMe)O^-$ and $(py)_2C(OH)O^-$ in **1** and **2**·MeCN, respectively, are unprecedented.

Magnetic properties

Solid-state, variable-temperature dc magnetic susceptibility (χ_m) studies were performed on powdered samples of compounds **1** and **2**. Plots of the product $\chi_m T$ and χ_m *vs.* temperature for **1** and **2** are shown in Figs. 3 and 4, respectively.

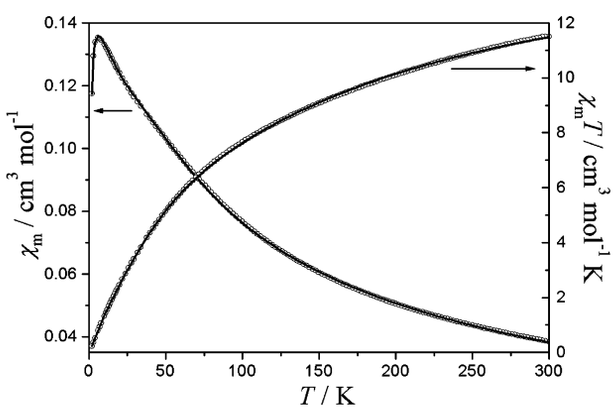

Fig. 3 Plots of $\chi_m T$ and χ_m *vs.* temperature for complex **1**. The solid lines are fits of the experimental data to the appropriate 2*J* model; see the text for the fitting parameters.

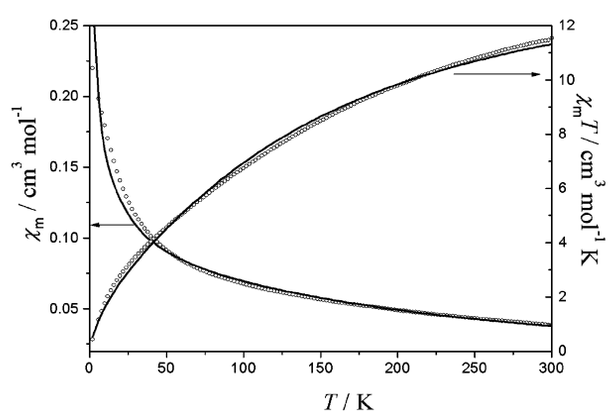

Fig. 4 Plots of $\chi_m T$ and χ_m *vs.* temperature for complex **2**. The solid lines are fits of the experimental data to the appropriate 2*J* model; see the text for the fitting parameters.

The $\chi_m T$ value of 11.47 cm^3 mol^{-1} K at 300 K for **1** is significantly below that (17.52 cm^3 mol^{-1} K for g = 2) expected for four non-interacting high-spin Fe^{III} ions. As the temperature

decreases, $\chi_m T$ gradually decreases, reaching a value of 0.23 cm^3 mol^{-1} K at 2.0 K. These data suggest operation of intramolecular antiferromagnetic interactions. The system obeys the Curie-Weiss law down to about 30 K, with $C = 15.56$ cm^3 mol^{-1} and $\Theta = -106.6$ K.The χ_m value increases with decreasing temperature, reaching a maximum at 5.9 K. Initial fitting approaches considering either $J_1 = J_2$ or $J_1 \neq J_2$ gave very poor results. Since high-spin Fe^{III} ions present no orbitally degenerate ground states, the possible operation of anisotropy can only originate from the highly distorted octahedral ligand environments of the metal centres resulting in single-ion zero-field splitting (ZFS). The effective spin Hamiltonian of the system, presented in eqn. (4),

$$\hat{H} = -2J_1\hat{S}_1\hat{S}_{1'} - 2J_2(\hat{S}_1\hat{S}_2 + \hat{S}_{1'}\hat{S}_{2'}) + D_1(\hat{S}_{z1}{}^2 + \hat{S}_{z1'}{}^2) + D_2(\hat{S}_{z2}{}^2 + \hat{S}_{z2'}{}^2) \quad (4)$$

corresponds to the scheme of exchange pathways shown in Scheme 3. Analytical expressions for eigenvalues and susceptibility can not be derived due to the ZFS terms. In order to calculate the energy levels and coupling constants, diagonalization of the full matrix has been carried out.[28] A satisfactory fit (not shown) was obtained only when $J_1 \neq J_2$ and $D_1 \neq D_2 \neq 0$; the best fit parameters were $J_1 = -11.0$ cm^{-1}, $J_2 = -4.6$ cm^{-1}, $D_1 = -3.6$ cm^{-1}, $D_2 = 0.8$ cm^{-1} with $g = 1.86$ and a residual $R = 3.67 \times 10^{-5}$. Although the molecular structure of **1** reveals a highly distorted octahedral environment around Fe(1) and Fe(1′), such a large D_1 value seems quite unrealistic for high-spin iron(III). The magnitude of this parameter, along with the poor quality of the fit at very low temperatures, led us to consider the possible presence of a small percentage of paramagnetic impurity. Fitting the experimental data with the theoretical expression derived from the above spin Hamiltonian, and including an additional parameter (ρ), to account for a small paramagnetic contribution to the magnetic susceptibility, improves the fit ($R = 7.47 \times 10^{-6}$), especially at very low temperatures, the fit parameters being: $J_1 = -13.0$ cm^{-1}, $J_2 = -4.8$ cm^{-1}, $D_1 = -0.9$ cm^{-1}, $D_2 \approx 0$, $\rho = 0.24\%$ with $g = 1.89$. This fit is shown as the solid lines in Fig. 3. The exchange parameters are almost unchanged, but the ZFS parameters have been optimized at more reasonable values for high-spin iron(III), thus supporting the assumption of the presence of a minute paramagnetic contribution (ρ = 0.24%). An energy-level diagram indicates that the first paramagnetic ($S = 1$) excited state is only 5.2 cm^{-1} above the $S = 0$ ground state. Thus, we can rationalize the relatively high χ_m value at 2 K (despite the diamagnetic ground state) as originating not only from the presence of a small paramagnetic contribution, but also from partial population of excited states, even at a very low temperature.

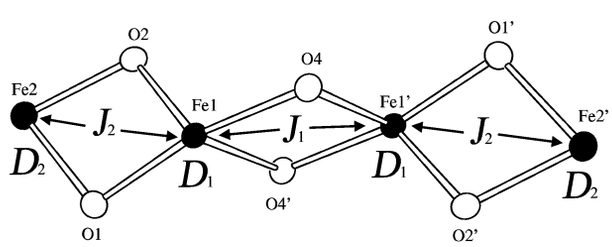

Scheme 3 Exchange interaction pattern for complex **1**.

The calculated J_1 and J_2 values are reasonable and consistent with the molecular structure of **1**. Fe(1) and Fe(1′) participate in a planar $[Fe_2(\mu\text{-}OR)_2]^{4+}$ subcore and the corresponding exchange interaction (J_1) is stronger than that (J_2) involving the Fe(1) ··· Fe(2) (and Fe(1′) ··· Fe(2′)) pairs which are involved in non-planar $[Fe_2(\mu\text{-}OR)(\mu\text{-}OR')]^{4+}$ subcores. Additionally, Fe(1) and Fe(1′) present the larger ZFS term, in accord with the more distorted coordination environment for these metal centres. The antiferromagnetic coupling between Fe(1) and Fe(1′) is weak ($J_1 = -13.0$ cm^{-1}) but does appear to be consistent with that reported for dinuclear complexes containing planar catecholato $[Fe_2(\mu\text{-}O_{catecholato})_2]^{4+}$ cores, for example $(Ph_4P)_2[Fe_2(cat)_4(H_2O)_2]$ ($J = -9.7$ cm^{-1} with the J value derived from a $-2JS_iS_j$ Hamiltonian formalism).[13] Generally the J_1 and J_2 values for **1** are in the range reported for dialkoxo-bridged iron(III) complexes.[34]

The room-temperature $\chi_m T$ product for complex **2** (11.55 cm^3 mol^{-1} K) is lower than expected for three uncoupled $S = 5/2$ Fe^{III} ions (13.14 cm^3 mol^{-1} K), indicating antiferromagnetic interactions. When the sample is cooled down, $\chi_m T$ decreases continuously and does not extrapolate to zero as the temperature approaches to zero. The susceptibility increases steadily with decreasing temperature reaching a value of 0.22 cm^3 mol^{-1} at 2.0 K and indicating a magnetic ground state, as expected for three $S = 5/2$ spins. The system obeys the Curie–Weiss law down to about 100 K, with $C = 18.05$ cm^3 mol^{-1} and $\Theta = -168.7$ K.

From a strict structural viewpoint, the Fe_3 triangle of **2** is scalene (Fe ··· Fe = 3.280, 3.411 and 3.441 Å). From the magnetochemical viewpoint we can consider the triangle as isosceles, taking into account the presence of single alkoxo-type bridges between Fe(1) and Fe(3), and Fe(2) and Fe(3), see Scheme 4. The experimental data were fitted by the theoretical equation derived from the appropriate effective spin Hamiltonian (eqn. (5)),

$$\hat{H} = -2J_1\hat{S}_1\hat{S}_2 - 2J_2(\hat{S}_1\hat{S}_3 + \hat{S}_2\hat{S}_3) \quad (5)$$

leading to a reasonable agreement; the fitting parameters were $J_1 = -7.1$ cm^{-1}, $J_2 = -4.7$ cm^{-1}, $g = 2.163$ ($R = 1.29 \times 10^{-3}$). Since the main superexchange pathways in **2** involve the *monoatomic* bridges O(1), O(2), O(4) and O(7), the relative J values are consistent with the molecular structure of the complex. The exchange interaction (J_2) between iron(III) atoms bridged by a single OR(R′) group is weaker than that (J_1) between metal ions bridged by two alkoxo-type oxygen atoms. The origin of the slight disagreement between the experimental data and calculated curves at low temperatures is unclear to us, and may stem from distortions of the iron(III) coordination spheres from octahedral geometries. However, efforts to simulate this behaviour by introducing zero-field splitting terms in the model, did not improve the fit.

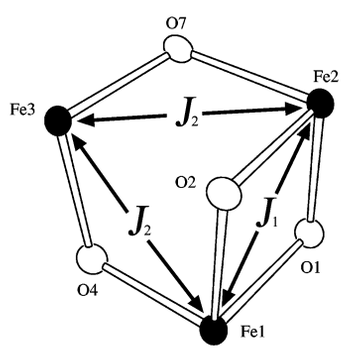

Scheme 4 Exchange interaction pattern for complex **2**.

The structure and magnetic properties of the anion of **2** are somewhat similar to those of the previously reported anion $[Fe_3(\mu_3\text{-}OMe)(\mu_2\text{-}OMe)_3(OMe)_3(dbm)_3]^-$, where the high-spin Fe^{III} ions are antiferromagnetically coupled with an $S = 1/2$ ground state.[35] Assumption of a C_{2v} point-group symmetry for the cluster led to a satisfactory reproduction of the observed magnetic behaviour with $g = 2.0$ and either $J = -5.3$ cm^{-1}, $J' = -7.7$ cm^{-1} or $J = -6.5$ cm^{-1}, $J' = -4.9$ cm^{-1}, where the spin-only Hamiltonian is defined as $\hat{H} = \Sigma_{i>j}(-2J_{i,j}S_iS_j)$ and J' is the unique coupling constant.

Table 4 Mössbauer parameters for complex **1**

Site	T/K	δ^a/mm s^{-1}	ΔE_Q/mm s^{-1}	$\Gamma_{1/2}{}^b$/mm s^{-1}	Area ratio^c (%)
Fe(1)	6	0.580(2)	1.306(8)	0.172(4)	50
Fe(1)	80	0.606(4)	1.308(9)	0.151(4)	50
Fe(1)	150	0.591(5)	1.28(1)	0.139(3)	50
Fe(1)	300	0.52(2)	1.27(5)	0.155(7)	50
Fe(2)	6	0.537(3)	0.927(8)	0.181(4)	50
Fe(2)	80	0.537(6)	1.00(1)	0.189(6)	50
Fe(2)	150	0.503(8)	1.02(2)	0.190(6)	50
Fe(2)	300	0.41(3)	1.05(6)	0.19(1)	50

^{a} Isomer shift referenced to iron foil at 300 K. ^{b} Width at half height. ^{c} Fixed values.

Mössbauer spectroscopy

The ^{57}Fe Mössbauer spectra of complex **1** were recorded at 6, 80, 150 and 300 K and are shown in Fig. 5. They consist of composite asymmetric doublets, that can be fitted with two quadrupole-split doublets (Lorentzian lines), with parameters (Table 4) typical of high-spin iron(III) in non-sulfur environments.[36,37] These parameters should correspond to the two Fe^{III} sites (Fe(1)/Fe(1′) and Fe(2)/Fe(2′)) present in the molecule of **1**. Site 1 (Fe(1)/Fe(1′)) has an NO_5 coordination sphere, while site 2 (Fe(2)/Fe(2′)) is characterized by an N_2O_4 set. In principle, as O atoms of the donor set are replaced by N atoms, a reduction of the isomer shift (δ) is expected; consequently, a higher δ value is expected for the O-richer coordination sphere of site 1. Also, since valence-electron contribution to the quadrupole splitting (ΔE_Q) is negligible for high-spin iron(III), the magnitude of ΔE_Q should reflect deviations from octahedral geometries. Thus, a higher ΔE_Q value is expected[37] for the severely distorted site 1. A further argument to this assumption ensues from the magnetic treatment, which clearly indicates a larger absolute value for the ZFS parameter of site 1 ($D_1 = -0.9$ cm^{-1}, $D_2 \approx 0$).

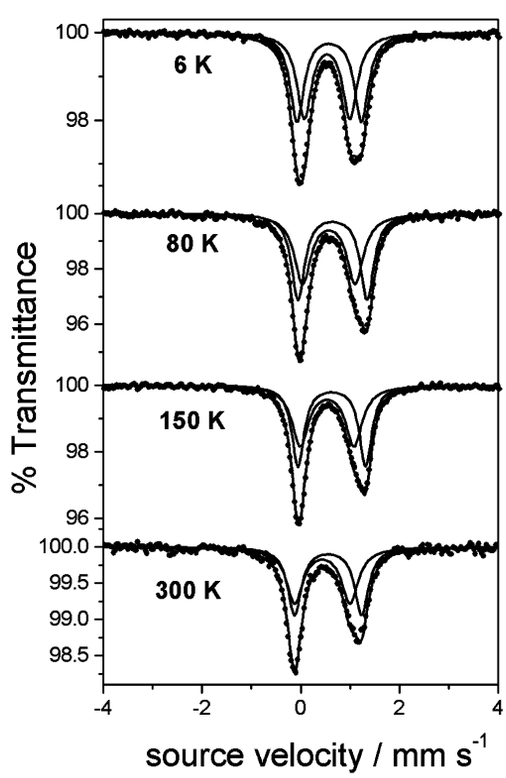

Fig. 5 Variable-temperature ^{57}Fe Mössbauer spectra of complex **1**. The solid line is a fit of the data with the two equal-area doublets shown. See Table 4 for the fitting parameters.

Due to the close proximity of the two quadrupole-split doublets, which is usual for high-spin iron(III), the relative areas of the two sites have been constrained to equality in order to avoid local minima without physical meaning. The results of the fits presented in Table 4 show that, at any temperature, the doublets corresponding to site 1 (Fe(1)/Fe(1′)) are, as expected, characterized by higher δ and ΔE_Q values. Values of δ decrease with increasing temperature, due to the second-order Doppler effect.[37] There is no clear trend in the thermal variation of the ΔE_Q parameter for site 1. For site 2, however, a slight increase of ΔE_Q with increasing temperature is observed.

The Mössbauer spectra of complex **2** at 80, 150 and 293 K (deposited as ESI,† Fig. S1) show an asymmetric doublet corresponding to high-spin iron(III) sites. In this case, however, the presence of three different iron sites (as evidenced by the molecular structure of the complex) makes deconvolution a much more difficult task, taking into account that, for high-spin iron(III), Mössbauer parameters are weakly sensitive to changes in coordination environment and symmetry. Consequently, the spectra have not been fitted with three iron sites. Characteristically, however, we can give the parameters obtained by fitting the 80 K Mössbauer spectrum with one (averaged) quadrupole split doublet: $\delta = 0.551$ mm s^{-1} $\Delta E_Q = 1.406$ mm s^{-1}, $\Gamma_{1/2} = 0.187$ mm s^{-1}.

Conclusions and perspectives

The initial use of the $(py)_2CO/H_2$dbcat "blend" in iron(III) chemistry has provided access to two new Fe clusters, one tetranuclear with a $[Fe_4(\mu_2\text{-}OR)_4(\mu_2\text{-}OR')_2]^{6+}$ core and the other trinuclear with a $[Fe_3(\mu_2\text{-}OR)_3(\mu_2\text{-}OR')]^{5+}$core. The various forms of $(py)_2CO$ and the dianionic dbcat^{2-} are ligated with a variety of coordination modes (Scheme 2), both bridging and terminal, thus attesting the great structural flexibility of the mixed-ligand system. Although both complexes have been found to possess low-spin ground states, they nevertheless suggest possibilities for other Fe_x species that might exist (*e.g.*, clusters containing the strongly coordinating inorganic anions NO_3^-, N_3^- and SO_4^{2-}) and which may have high-spin ground states. In addition, they provide encouragement for believing that a variety of M^{II}_x and M^{III}_x clusters (M^{II} = Co^{II}, Ni^{II} M^{III} = Cr^{III}, Mn^{III}) should also be accessible with this ligand "blend", leading to new topologies not seen or accessible with the individual ligands. Such species will be interesting to study, considering how exciting their magnetic properties could be; for example Mn^{III} complexes are worthy of study because in Mn^{III}_x cluster chemistry $S = 0$ or $S = 1/2$ are the exception rather than the rule. Further work with Fe^{III} and parallel studies with Mn^{III}, Co^{II} and Ni^{II} employing the $(py)_2CO/H_2$dbcat "blend" are currently in progress.

Acknowledgements

A. K. B. thanks the European Community for partial support through a postdoctoral grant within the framework of the TMR contract FMRX- CT980174.

References

1 D. M. Kurtz, Jr., *J. Biol. Inorg. Chem.*, 1997, **2**, 159; L. Que, Jr., *J. Chem. Soc., Dalton Trans.*, 1997, 3933; P. Nordlund and H. Eklund, *Curr. Opin. Struct. Biol.*, 1995, **5**, 758.

2 E. C. Theil, in *Handbook of Metalloproteins*, ed. A. Messerschmidt, R. Huber, T. Poulos and K. Wieghardt, Wiley, Chichester, 2001, pp. 771–781.

3 E. K. Brechin, M. J. Knapp, J. C. Huffman, D. N. Hendrickson and G. Christou, *Inorg. Chim. Acta*, 2000, **297**, 389; W. Micklitz and S. J. Lippard, *Inorg. Chem.*, 1988, **27**, 3067; S. M. Gorun and S. J. Lippard, *Nature*, 1986, **319**, 666.

4 A. K. Powell, S. L. Heath, D. Gatteschi, L. Pardi, R. Sessoli, G. Spina, F. D. Giallo and F. Pieralli, *J. Am. Chem. Soc.*, 1995, **117**, 2491.

5 C. Benelli, J. Cano, Y. Journaux, R. Sessoli, G. A. Solan and R. E. P. Winpenny, *Inorg. Chem.*, 2001, **40**, 188; D. Gatteschi, R. Sessoli and A. Cornia, *Chem. Commun.*, 2000, 725, and references therein; A. L. Barra, A. Caneschi, A. Cornia, F. Fabrizi de Biani, D. Gatteschi, C. Sangregorio, R. Sessoli and L. Sorace, *J. Am. Chem. Soc.*, 1999, **121**, 5302.

6 For excellent reviews, see: D. Gatteschi and R. Sessoli, *Angew. Chem., Int. Ed.*, 2003, **42**, 268; G. Christou, D. Gatteschi, D. N. Hendrickson and R. Sessoli, *MRS Bull.*, 2000, **25**, 1.

7 E. K. Brechin, C. Boskovic, W. Wernsdorfer, J. Yoo, A. Yamaguchi, E. C. Sañudo, T. R. Concolino, A. L. Rheingold, H. Ishimoto, D. N. Hendrickson and G. Christou, *J. Am. Chem. Soc.*, 2002, **124**, 9710, and references therein; M. Soler, S. K. Chandra, D. Ruiz, E. R. Davidson, D. N. Hendrickson and G. Christou, *Chem. Commun.*, 2000, 2417, and references therein.

8 A. K. Boudalis, N. Lalioti, G. A. Spyroulias, C. P. Raptopoulou, A. Terzis, A. Bousseksou, V. Tangoulis, J.-P. Tuchagues and S. P. Perlepes, *Inorg. Chem.*, 2002, **41**, 6474; A. K. Boudalis, N. Lalioti, G. A. Spyroulias, C. P. Raptopoulou, A. Terzis, V. Tangoulis and S. P. Perlepes, *J. Chem. Soc., Dalton Trans.*, 2001, 955; A. K. Boudalis, V. Tangoulis, C. P. Raptopoulou, A. Terzis, J.-P. Tuchagues and S. P. Perlepes, *Inorg. Chim. Acta*, 2003, submitted.

9 For a review, see: G. S. Papaefstathiou and S. P. Perlepes, *Comments Inorg. Chem.*, 2002, **23**, 249.

10 Recent literature: G. S. Papaefstathiou, A. Escuer, M. Font-Bardia, S. P. Perlepes, X. Solans and R. Vicente, *Polyhedron*, 2002, **21**, 2027; G. S. Papaefstathiou, S. P. Perlepes, A. Escuer, R. Vicente, M. Font-Bardia and X. Solans, *Angew. Chem., Int. Ed.*, 2001, **40**, 884; G. S. Papaefstathiou, A. Escuer, C. P. Raptopoulou, A. Terzis, S. P. Perlepes and R. Vicente, *Eur. J. Inorg. Chem.*, 2001, 1567; G. S. Papaefstathiou, A. Escuer, R. Vicente, M. Font-Bardia, X. Solans and S. P. Perlepes, *Chem. Commun.*, 2001, 2414; C. J. Milios, E. Kefalloniti, C. P. Raptopoulou, A. Terzis, R. Vicente, N. Lalioti, A. Escuer and S. P. Perlepes, *Chem. Commun.*, 2003, 819.

11 Recent literature: M.-L. Tong, S.-L. Zheng, J.-X. Shi, Y.-X. Tong, H. K. Lee and X.-M. Chen, *J. Chem. Soc., Dalton Trans.*, 2002, 1727; M. G. Barandika, Z. Serna, R. Cortes, L. Lezana, M. K. Urtiaga, M. I. Ariortua and T. Rojo, *Chem. Commun.*, 2001, 45.

12 J. Woltz, B. L. Westcott, G. Grundwell, M. Zeller, A. D. Hunter and S. O. Sommerer, *Acta Crystallogr., Sect. E*, 2002, **58**, m609.

13 V. A. Grillo, G. R. Hanson, D. Wang, T. W. Hambley, L. R. Gahan, K. S. Murray, B. Moubaraki and C. J. Hawkins, *Inorg. Chem.*, 1996, **35**, 3568.

14 O. Carugo, C. Bisi Castellani, K. Djinovic and M. Rizzi, *J. Chem. Soc., Dalton Trans.*, 1992, 837.

15 S. C. Shoner and P. P. Power, *Inorg. Chem.*, 1992, **31**, 1001.

16 S. R. Boone, G. H. Purser, H.-R. Chang, M. D. Lowery, D. N. Hendrickson and C. G. Pierpont, *J. Am. Chem. Soc.*, 1989, **111**, 2292.

17 L. Que, Jr. and R. Y. N. Ho, *Chem. Rev.*, 1996, **96**, 2607; K. N. Raymond, *Coord. Chem. Rev.*, 1990, **105**, 135.

18 B. F. Matzanke, G. Muller-Matzanke and K. N. Raymond, in *Iron Carriers and Iron Proteins*, ed. T. M. Loehr, Physical Bioinorganic Series, VCH Publishers, New York, 1989, pp. 1–121.

19 S. W. Taylor, J. D. Cashion, L. J. Brown, C. J. Hawkins and G. R. Hanson, *Inorg. Chem.*, 1995, **34**, 1487; S. W. Taylor, G. W. Luther and J. H. Waite, *Inorg. Chem.*, 1994, **33**, 5819; K. N. Raymond, G. Muller and B. F. Matzanke, *Top. Curr. Chem.*, 1984, **123**, 49.

20 For example, see: D. Zirong, S. Bhattacharya, J. K. McCusker, P. M. Hagen, D. N. Hendrickson and C. G. Pierpont, *Inorg. Chem.*, 1992, **31**, 870; H. G. Jang, D. D. Cox and L. Que, Jr, *J. Am. Chem. Soc.*, 1991, **113**, 9200.

21 R. E. P. Winpenny, *J. Chem. Soc., Dalton Trans.*, 2002, 1.

22 E. Diamantopoulou, C. P. Raptopoulou, A. Terzis, V. Tangoulis and S. P. Perlepes, *Polyhedron*, 2002, **21**, 2117; N. Lalioti, C. P. Raptopoulou, A. Terzis, A. E. Aliev, I. P. Gerothanassis, E. Manessi-Zoupa and S. P. Perlepes, *Angew. Chem., Int. Ed.*, 2001, **40**, 3211; G. S. Papaefstathiou, C. P. Raptopoulou, A. Tsohos, A. Terzis, E. G. Bakalbassis and S. P. Perlepes, *Inorg. Chem.*, 2000, **39**, 4658.

23 X-SHAPE: Crystal Optimisation for Numerical Absorption Corrections, Revision 1.01, Stoe & Cie, Darmstadt, Germany, 1996.

24 G. M. Sheldrick, SHELXS-97, Program for Crystal Structure Solution, University of Göttingen, Germany, 1997.

25 G. M. Sheldrick, SHELXL-97, Program for the Refinement of Crystal Structures from Diffraction Data, University of Göttingen, Germany, 1997.

26 *International Tables for Crystallography*, Kluwer Academic Publishers, Dordrecht, The Netherlands, 1992, Vol. C, Tables 4.2.6.8 and 6.1.1.4.

27 ORTEP32 for Windows: L. J. Farrugia, *J. Appl. Crystallogr.*, 1997, **30**, 565.

28 J. M. Clemente-Juan, C. Mackiewicz, M. Verelst, F. Dahan, A. Bousseksou, Y. Sanakis and J.-P. Tuchagues, *Inorg. Chem.*, 2002, **41**, 1478.

29 F. James and M. Roos, MINUIT Program, a System for Function Minimization, and Analysis of the Parameters Errors and Correlations, Comput. Phys. Commun., 1975, **10**, 345.

30 K. Lagarec, Recoil, Mössbauer Analysis Software for Windows, http://www.physics.uottawa.ca/~recoil.

31 E. C. Constable, *Metals and Ligand Reactiviy*, VCH, Weinheim, Germany, 2nd edn., 1996, pp. 46–48, 57—59.

32 R. A. Coxall, S. G. Harris, D. K. Henderson, S. Parsons, P. A. Tasker and R. E. P. Winpenny, *J. Chem. Soc., Dalton Trans.*, 2000, 2349.

33 A. W. Addison, T. N. Rao, J. Reedijk, J. van Rijn and G. C. Verschoor, *J. Chem. Soc., Dalton Trans.*, 1984, 1349.

34 F. Le Gall, F. Fabrizi de Biani, A. Caneschi, P. Cinelli, A. Cornia, A. C. Fabretti and D. Gatteschi, *Inorg. Chim. Acta*, 1997, **262**, 123; S. M. Gorun and S. J. Lippard, *Inorg. Chem.*, 1991, **30**, 1625; R. Werner, S. Ostrovsky, K. Griesar and W. Haase, *Inorg. Chem.*, 2001, **326**, 78.

35 A. Caneschi, A. Cornia, A. C. Fabretti, D. Gatteschi and W. Malavasi, *Inorg. Chem.*, 1995, **34**, 4660.

36 K. S. Murray, *Coord. Chem. Rev.*, 1974, **12**, 1.

37 N. N. Greenwood and T. C. Gibbs, *Mössbauer Spectroscopy*, Chapman and Hall, London, 1971.